A High-Performance OFDMA PON System Architecture and Medium Access Control

Maria C. Yuang, *Senior Member, IEEE, Member, OSA*, Po-Lung Tien, *Member, IEEE*, Dar-Zu Hsu, Shing-Yu Chen, Chia-Chien Wei, Ju-Lin Shih, *Member, IEEE*, and Jyehong Chen

***Abstract*—Orthogonal frequency-division multiplexing (OFDM) passive optical network (PON) has been considered to be a promising next-generation broadband wired access solution. However, based on the current tree-based architecture, existing OFDM PON systems face severe challenges when increasing the scalability and data-rate performance. In this paper, we propose a high-performance *virtual-tree* orthogonal frequency-division multiple access PON system (VTOPS). With the virtual-tree architecture and coupled with the use of inexpensive direct modulation, VTOPS features high reliability, scalability, spectrum efficiency, and cost effectiveness all at once. For governing the flexible/fair access and dynamic allocation of bandwidth, VTOPS incorporates a rate-based medium access control (MAC) scheme. The MAC scheme performs dynamic rate adjustment using a neural-fuzzy system. By adjusting the system parameters, the MAC scheme can achieve a wide range of delay and fairness performance under a variety of traffic patterns. Finally, we show both theoretical and experimental results to demonstrate that, by applying the power pre-emphasis algorithm and adaptive subchannel modulation, VTOPS achieves 40 Gb/s downlink and 40 Gb/s uplink transmissions, using low-cost 10 GHz directly modulated lasers.**

***Index Terms*—Direct modulation, medium access control (MAC), orthogonal frequency-division multiple access (OFDMA), passive optical network (PON).**

Manuscript received November 14, 2011; revised December 30, 2011, January 21, 2012; accepted January 21, 2012. Date of publication February 03, 2012; date of current version April 06, 2012. This work was supported in part by the National Science Council, Taiwan, under Grant 97-2221-E-009-061-MY3, and in part by the Information and Communications Research Laboratories/Industrial Technology Research Institute Joint Research under Contract 3000291254.

M. C. Yuang is with the Department of Computer Science and Information Engineering, National Chiao Tung University, Hsinchu 300, Taiwan (e-mail: mcyuang@csie.nctu.edu.tw).

P.-L. Tien is with the Department of Electrical Engineering, National Chiao Tung University, Hsinchu 300, Taiwan (e-mail: polungtien@gmail.com).

D.-Z. Hsu is with the Department of Photonics, National Chiao Tung University, Hsinchu 300, Taiwan, and also with the Information and Communications Research Laboratories, Industrial Technology Research Institute, Hsinchu 300, Taiwan (email: sparkle@itri.org.tw).

S.-Y. Chen is with the Information and Communications Research Laboratories, Industrial Technology Research Institute, Hsinchu 300, Taiwan (e-mail: star.1585@yahoo.com.tw).

C.-C. Wei is with the Department of Photonics, National Sun Yat-sen University, Kaohsiung 804, Taiwan (e-mail: mgyso.wei@gmail.com).

J.-L. Shih was with the Department of Computer Science and Information Engineering, National Chiao Tung University, Hsinchu 300, Taiwan. He is now with Compal Communications, Inc., Taipei 114, Taiwan (e-mail: julin@csie.nctu.edu.tw).

J. Chen is with the Department of Photonics, National Chiao Tung University, Hsinchu 300, Taiwan (e-mail: jchen@mail.nctu.edu.tw).

Color versions of one or more of the figures in this paper are available online at http://ieeexplore.ieee.org.

Digital Object Identifier 10.1109/JLT.2012.2186954

I. Introduction

To support bandwidth-hungry applications and to seamlessly provide a multitude of broadband services over an IP network, passive optical networks (PONs) [1], [2]—with immense bandwidth and low-cost fiber infrastructure—have been considered to be one of the most promising broadband access solutions. A PON is a point-to-multipoint tree-structured network, where the optical line terminal (OLT) at the central office is connected to a number of optical network units (ONUs) at end user premises via a passive optical device. Serving as the ultimate broadband wired access solution, next-generation PON systems are expected to provide high scalability and bandwidth (e.g., 40 Gb/s and beyond) at reasonably low cost.

Recently, there have been significant developments of three classes of PON systems: time-division multiple access (TDMA) [1], [2], wavelength-division multiplexing (WDM) [1], [2], and orthogonal frequency-division multiple access (OFDMA) [1], [3]–[5]. In these systems, while downstream data are simply broadcast from OLT to all ONUs, upstream data from ONUs to OLT are multiplexed in the domain of time, wavelength, frequency, or the combination of earlier. To this end, PON systems are equipped with medium access control (MAC) to ensure collision-free access of upstream bandwidth and to provide dynamic bandwidth allocation, ultimately to achieve access fairness and maximal throughput.

In a TDMA PON, the transmission is based on the simple nonreturn-to-zero ON–OFF keying (NRZ-OOK) modulation. However, the increasing demand for ultrahigh data rates of $40+$ Gb/s poses real challenges to the current designs of TDM PON systems. First, to increase the NRZ-OOK data rate, the traditional tree-and-branch architecture creates power budget (receiver sensitivity) and scalability problems resulting from the high insertion loss of the splitter. To combat the problems, current systems have to use expensive optical amplification devices (semiconductor optical amplifier or erbium-doped fiber amplifier). Second, to support a transmission rate of $40+$ Gb/s, TDMA PON systems require expensive and sophisticated high-speed optical components (e.g., laser, external modulator, and burst-mode receiver). Third, because the fiber chromatic dispersion (CD) tolerance degrades in proportion to the square of the bandwidth, supporting a data rate of $40+$ Gb/s severely limits the fiber transmission distance.

Contrastingly, a WDM PON system uses a multiplexer/demultiplexer at the distribution end, thereby allowing a dedicated wavelength to be allocated to each ONU, and achieving superior per-user throughput. Nevertheless, WDM PON systems

face their own set of challenges. First, a WDM PON system has to satisfy the colorless requirement, namely transmitting on a designated wavelength without using a color-specific device. To meet the need, existing technologies include the use an optical tunable laser at each ONU, or the provision of a wavelength-specific light source by OLT. Both techniques are unfortunately overly complex and expensive, thus remaining a technical bottleneck. Furthermore, such a design yields inflexible bandwidth allocation on a subwavelength granularity basis, which gives rise to a scalability problem. From these aforementioned considerations, it is apparent that to provide high bandwidth and scalability while keeping costs reasonably low, the architecture and implementation of current PON systems need to be fundamentally redesigned.

II. OFDMA-PON Challenges

Thanks to advances in digital signal processing technology, one such prominent candidate for next-generation PONs is OFDMA-PON [1], [3], [5], [6]. Orthogonal frequency-division multiplexing (OFDM) PON systems achieve high data rates by adopting higher order quadrature-amplitude modulation (QAM) for each subcarrier. OFDM is known for its high spectral efficiency, which brings a benefit of a lower optical-component bandwidth requirement [5]. For example, based on 16 QAM, one can achieve a 40 Gb/s data rate by using a low-bandwidth 10 GHz optical transceiver. Due to the lower bandwidth usage, as a result, the optical OFDMA system not only increases the transmission data rate in a cost-effective manner, but it is also more immune to both CD and polarization mode dispersion. Additionally, compared to WDM PONs, OFDMA PON systems allow far more dynamic and fine-grained (subcarrier-based) bandwidth allocation.

Despite these advantages over TDM and WDM PONs, OFDMA PON systems face two hurdles. First, the current tree topology poses two critical problems. When two lasers that are physically located at two different ONUs operate at closely spaced frequencies, their interference creates an unwanted signal beating noise, called optical-beat-interference (OBI) noise. The OBI results in severe signal degradation after the photodetector at the optical receiver end. Qian *et al*. [7] proposed a source-free ONU light source to solve the OBI problem, but at the expense of high complexity and cost. Furthermore, when a high splitting-ratio splitter is used to scale up the number of connected ONUs, a tree-topology OFDMA system undergoes considerable optical power fading and optical signal-to-noise ratio (OSNR) degradation. Such OSNR degradation prevents the system from taking advantage of high-order QAM. Therefore, the current tree-based topology can be challenging for OFDMA PON systems. At the same time, such an architecture change brings about the need for redesigning the existing MAC schemes that cater for tree-based PON systems.

The second challenge involves the overall system cost. Recently, a number of OFDM PON systems have been proposed and demonstrated based on the external-modulation technique, e.g., using Mach–Zehnder modulator (MZM) [8]. MZM-based approaches generate chirp-free single-sideband [8] optical signals. As a result, they achieve superior optical transmission performance without the power-fading problem, however, at the expense of higher cost. A viable cost-effective alternative is the direct-modulation technique. Examples are distributed feedback directly modulated lasers (DML), and electro-absorption-modulated lasers (EML). As opposed to the MZM approach, they generate positive-chirp double-sideband (DSB) optical signals. Unfortunately, after single-mode-fiber (SMF) transmissions, fiber dispersion and frequency chirp cause each signal sideband to experience different phase shifts, resulting in severe power fading [5]. The primary goal of this paper is to design and experiment with a cost-effective high-performance OFDMA-PON system (and its MAC scheme) to overcome these two hurdles.

In this paper, we propose a *virtual-tree* OFDMA PON system (VTOPS). Rather than using a splitter, VTOPS employs a remote node (RN) that connects ONUs to OLT via a number of bypassable circulators in a point-to-point manner, forming a so-called virtual-tree topology. With the virtual-tree architecture and coupled with the use of inexpensive direct modulation, VTOPS features high reliability, scalability, spectrum efficiency, and cost effectiveness all at once. In addition, VTOPS incorporates a rate-based MAC scheme for governing the flexible/fair access and dynamic allocation of bandwidth. The scheme embodies dynamic rate adjustment being implemented by a neural-fuzzy system. The MAC scheme, as will be shown, achieves low delay and high fairness under a variety of traffic patterns.

Furthermore, we justify through a theoretical analysis that the power-fading problem caused by the use of DML/EML can be effectively overcome by applying a power pre-emphasis algorithm together with adaptive subcarrier modulation. Finally, we demonstrate both theoretical and experimental results to show that, VTOPS achieves 40 Gb/s downlink and 40 Gb/s uplink transmissions, via the same fiber trunk, using a 10 GHz bandwidth EML and DML.

The remainder of this paper is organized as follows. In Section III, we present the architecture of VTOPS. In Section IV, we describe the neural-fuzzy rate-based MAC system. In Section V, we provide the theoretical analysis of DML and EML transmissions. In Section VI, we demonstrate the experimental setup and results. Finally, concluding remarks are given in Section VII.

III. VTOPS Architecture

VTOPS connects N ONUs to OLT through a trunk fiber and an RN, as shown in Fig. 1. The RN consists of one regular circulator and N three-port bypassable circulators [9] each of which connects to an ONU via one short section of feeder fiber. Without looking into the internal structure of the RN, VTOPS appears to have a tree topology like existing PONs. However, with the circulators in RN, the system transports data in a point-to-point manner from OLT to the first, second ONU sequentially until the last ONU and back to OLT. Such a topology is referred to as a *virtual tree*. Notice that, the structure differs from a ring in that the downstream traffic starts from OLT and ends at ONU_N, whereas the upstream traffic starts from ONU_1 and ends at OLT. Within the RN, if an ONU (and

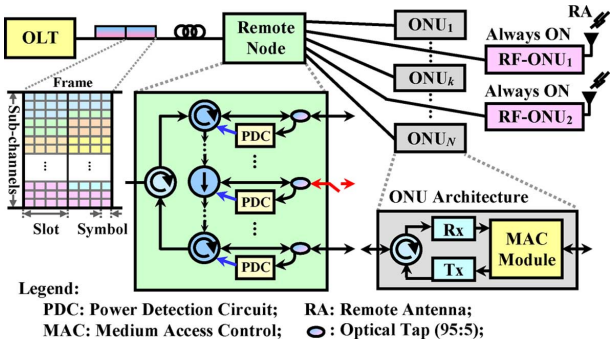

Fig. 1. VTOPS architecture.

its feeder fiber) is in working condition, its power detection circuit checks the power level from the feeder fiber and drives the corresponding bypassable circulator to the normal mode. When an ONU or feeder fiber fails, the corresponding bypassable circulator is notified of a loss of signal, and switches to the "bypass" mode.

In VTOPS, the bandwidth is accessed on a frame basis (see Fig. 1). Each frame is divided into a number of data and control OFDM subchannels. While the data subchannels carry payload information, the control subchannels convey the assignment map of data subchannels and access-control information. Each subchannel is further subdivided in the time domain into slots each of which is an integral number of OFDM symbols in length. With OFDMA, each ONU can access a number of slots (per frame) belonging to the same or different subchannels. The allocation of slots for each ONU is governed by its MAC module described in the next section.

With this virtual-tree topology, downstream and upstream data flow in VTOPS differently from that in existing PONs. Basically, both downstream and upstream data follow the same path within the system. OLT first passes the downstream OFDM signal to ONU_1 through the regular circulator at the RN. The ONU_1's MAC module performs downstream traffic extraction if its MAC address matches with the destination address. The ONU, then transmits data on a number of slots according to its MAC, and updates the control subchannels. Together with the remaining downstream data, the combined OFDMA signal is modulated and optically transmitted to the next ONU, ONU_2. The same operation repeats at ONU_2 and all downstream ONUs. Finally, when the data reach the last ONU (ONU_N), the aggregated upstream data are modulated on the optical transmitter and are transported back to OLT through the RN and trunk fiber. It is worth noting that in VTOPS, OLT and the last ONU are required to be equipped with more expensive EML to facilitate longer distance (20 km) transmissions; and all other ONUs only need inexpensive DML for transmissions of a shorter distance (5 km).

The virtual-tree architecture of VTOPS brings about several significant advantages. First, facilitated with the RN using bypassable circulators, VTOPS ensures high robustness against breakdowns and power-offs of ONU's. Notice that VTOPS is referred to as a passive system due to the fact that, compared to active access systems, VTOPS requires relatively small power to drive bypassable circulators to different modes. Second, because the signal is electrically regenerated at every ONU, the signal integrity can be maintained without using amplifiers. As a result, VTOPS is highly scalable with an increasing ONU number, and free from the power budget problem. Third, due to low loss between ONUs, the received signal is of relatively high OSNR. The fact enables VTOPS to employ high-order QAM formats and, thus, achieve high spectrum efficiency.

Nevertheless, VTOPS exhibits some disadvantages. First, the system incurs additional latency from the first to the last ONUs. However, with 32 ONUs that is 5 km apart from each adjacent one, the total delay is as small as 0.8 ms, which is tolerable for real-time applications. Second, for fiber-to-the-home systems, the ONUs at home may frequently be shut down. For the downstream data, a sequence of powered-off ONUs (being in the bypass mode) results in the deterioration of signal integrity. To solve the problem, a viable solution can be the inclusion of RF-ONUs that support radio over fiber (RoF) [5]. Notice that, unlike home ONUs, RF-ONUs are required to remain operational at all times. This fact brings significant benefit of ensuring signal integrity.

IV. Neural-Fuzzy Rate-Based MAC

In this section, we first introduce the basic neural-fuzzy approach that is known for resolving nonlinear complex system problems. We then present the basic rate-based MAC scheme, and the neural-fuzzy rate-based MAC system at each ONU. Finally, we demonstrate via simulation results the performance of the MAC scheme on the access delay and fairness of ONUs as the functions of major system parameters.

A. Neural-Fuzzy Approach

Pure-fuzzy control [10], which has been used to identify nonlinear systems, facilitates a *reasoning* capability by means of a set of fuzzy if–then rules. The fuzzy rules are usually obtained by heuristic observations and experiences of human experts. However, such a pure fuzzy system is impractical for problems (e.g., a nonlinear inverse problem in our case) where the fuzzy rules are unattainable. A neural network [11], on the other hand, is a computational learning model that consists of an interconnected group of neurons that are updated through a *learning* phase until the system reaches its equilibrium state of the objective function. By combining the strengths of neural-network's learning and fuzzy-system's reasoning, the neural-fuzzy approach [12]–[14] has been successfully used to solve complex nonlinear problems [14]. Numerous neural-fuzzy models [12]–[14] have been proposed. While most of them feature offline learning under static system scenarios, the self-constructing neural inference network (SONFIN) [14] was shown capable of managing dynamic systems. It is, thus, used as the basic model for our MAC system described next.

B. Neural-Fuzzy Rate-Based MAC System

Recall that the upstream OFDM frames pass from the first ONU to the last and then to OLT. At each ONU, its MAC scheme (or module) determines the total number of slots to be accessed in each frame in accordance with the number of *permits* the ONU has. As shown in Fig. 2(a), the permits are generated periodically at a rate, referred to as the permit rate (PR), and

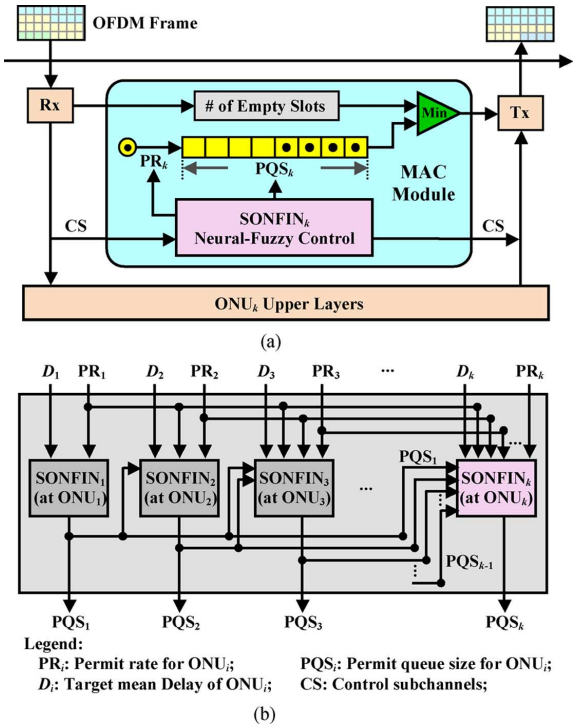

Fig. 2. Neural-fuzzy rate-based MAC. (a) Neural-fuzzy rate-based MAC module at ONU_k. (b) SONFIN-based neural-fuzzy MAC—a global view.

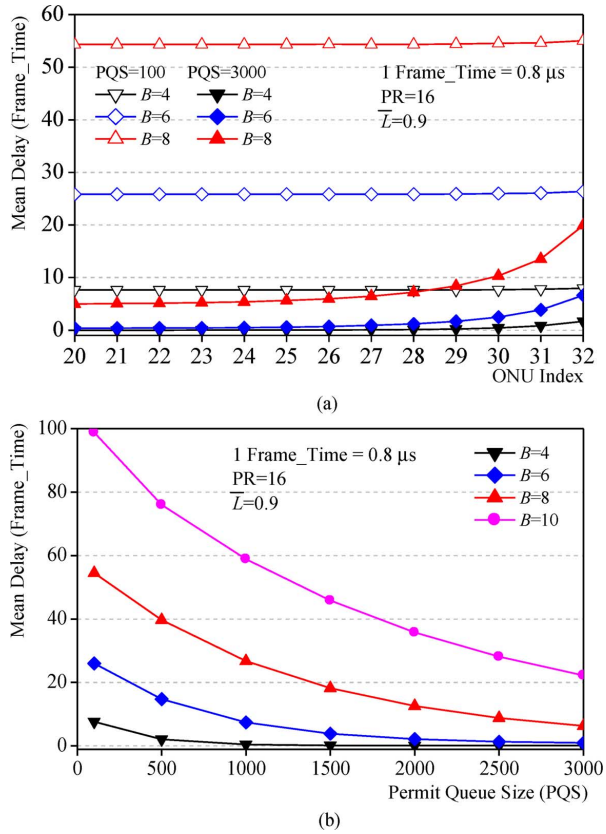

Fig. 3. Simulation results of MAC on mean delay and delay fairness. (a) Impact of PQS on mean delay and delay fairness. (b) Mean delay under different PQS settings.

added in the finite-size permit queue. Since the size of the permit queue (PQS) is finite, new permits arriving to a full permit queue are lost. Accordingly, the access of slots is solely dependent on the two system parameters—PR and PQS. The greater the PR and PQS, the higher the access rate and maximum burst length, respectively. Each ONU is, then, allowed to transmit p slots, where p takes the smaller value between the total number of permits in the queue and the empty slots in the current frame. After the transmissions, p permits are, then, removed from the permit queue. Notice that, the number of available permits can simply be implemented as a counter with an upper limit. Generation and removal of permits correspond to the addition and subtraction of the counter, respectively. The key problem that remains unresolved is the determination of the two system parameters, PR and PQS.

A higher PR allows an ONU to transmit a greater mean number of slots, while a higher PQS provides the ONU to transmit a larger burst of slots within a slot time. Both cases result in fewer empty slots to be passed and accessed by the following ONU. Thus, the settings of PR and PQS at each ONU not only directly affect the throughput and delay performance of itself, but also the performance of all ONUs that are downstream from it. Accordingly, the determination of PR and PQS has to be considered from a global perspective—with all ONUs' system parameters taken into account simultaneously. Therefore, the real challenge to the design of the MAC system lies in the joint determination of the permit parameters (PRs and PQSs) for all ONUs subject to minimizing the delay and maximizing the throughput of all ONUs simultaneously.

To meet this challenge, we have proposed a SONFIN-based neural-fuzzy control for each ONU, as illustrated in Fig. 2(b).

Recall that the mean delay D of an ONU is solely dependent on the PQS and PR of the ONU and all PQSs and PRs of all preceding ONUs. For example, for ONU_k, the mean delay D_k of ONU_k can be expressed as a function of these parameters, i.e.,

$$D_k = f_k(\mathrm{PR}_1, \ldots, \mathrm{PR}_{k-1}, \mathrm{PR}_k; \mathrm{PQS}_1, \ldots, \mathrm{PQS}_{k-1}, \mathrm{PQS}_k). \quad (1)$$

Function f_k can be best explained from the system results shown in Fig. 4(a). For example, for ONU_{30} $(k = 30)$, in order to achieve a delay $D = 5$, f_{30} is the pink curve shown in Fig. 4(a). In this example, PR values are the same among all ONUs.

Assume that PRs/PQSs of all preceding ONUs are made available at ONU_k. (Notice that, the set of information can be passed downstream through OFDM control subchannels). For ONU_k with a given PR_k, the determination of PQS_k subject to meeting the delay requirement D_k becomes an inverse (nonlinear) problem. That is

$$\mathrm{PQS}_k = f_k^{-1}(D_k)|_{(\mathrm{PR}_1,\ldots,\mathrm{PR}_{k-1};\mathrm{PQS}_1,\ldots,\mathrm{PQS}_{k-1};\mathrm{PR}_k)}. \quad (2)$$

Notice that, by the same token, with a given PQS_k, PR_k can be determined as: $\mathrm{PR}_k = f_k^{-1}(D_k)|_{(\mathrm{PR}_1,\ldots,\mathrm{PR}_{k-1};\mathrm{PQS}_1,\ldots,\mathrm{PQS}_{k-1};\mathrm{PQS}_k)}$. As will be shown in the next subsection, the mean delay is as sensitive to the PQS value as to the PR value. Since PQS is taken as an integer value

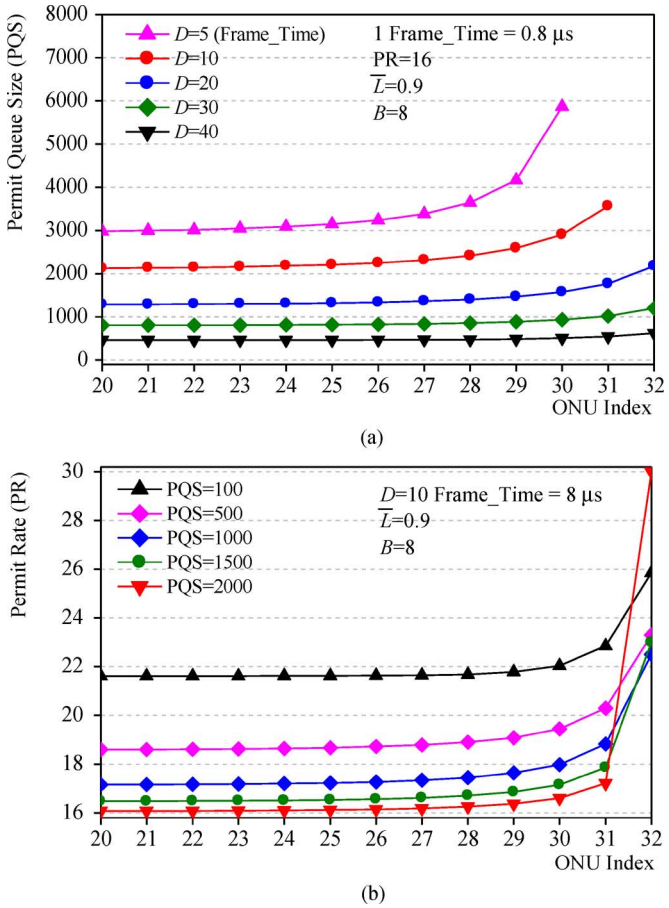

Fig. 4. Simulation results of the neural-fuzzy rate-based MAC system. (a) PQS settings for ONUs satisfying different delay requirements. (b) PR/PQS settings for ONUs satisfying a given delay requirement.

(whereas PR is taken as a real-number value), for simplicity, we adopt the changing of the PQS value under a fixed PR, in (2) and throughout the rest of this section.

Therefore, to optimize the PR and PQS values of all ONU subject to minimizing the delay and achieving delay fairness, we employ the SONFIN-based neural-fuzzy control to solve the inverse function f^{-1} in (2) using its learning and reasoning capabilities. That is, as shown in Fig. 2(b), given a $2k$-tuple input, $(D_k; \mathrm{PR}_1, \ldots, \mathrm{PR}_{k-1}; \mathrm{PQS}_1, \ldots, \mathrm{PQS}_{k-1}, \mathrm{PR}_k)$, SONFIN_k is to generate one output, PQS_k. The determination of PQS (or PR) operates in two phases: offline pretraining, and online computation/training. In the offline pretraining phase, we collect and use a representative set of training data from simulation results to perform the learning of fuzzy if–then rules. Each training data include a $2k$-tuple input and one output, as described previously. In the online computation phase, per every time period, with PRs and PQSs of all ONUs (PR_i and PQS_i, for $i = 1$ to $k-1$) fed into SONFIN_k, together with its D_k and PR_k, SONFIN_k in turn outputs the PQS_k value. The $\mathrm{PR}_k/\mathrm{PQS}_k$ values are then used by the MAC module [see Fig. 2(a)] to manage the number of permits for governing the slot access within the time period. It is worth noting that, during the online phase, the SONFIN system continues learning and adjusting its internal parameters to adapt to the varying traffic environment.

C. Simulation Results

We first carried out simulation of the basic MAC scheme to examine the mean delay and delay fairness performance with respect to different PQS settings and traffic burstiness. (The rationale behind using different PQS instead of PR settings is two-fold. First, PQS is an integer value that is simpler for adjustment. In addition, system performance is as sensitive to the PQS settings as to the PR settings.) In the simulations, VTOPS has N ONUs ($N = 32$) and operates at a rate of 10 Gb/s. All ONUs share a total of 512 OFDM data-subchannel slots on a Frame_Time basis. Each OFDM slot is 16 bits long, thus making a Frame_Time being 0.8 μs (16*512/10G) in length.

Data arrivals for all ONUs are assumed to be identical. Let $\bar{L}$ represent the aggregate mean offered load (data slots/Frame_Time). Then, the mean offered load from each ONU, denoted as $\bar{L}_o$, is $(512/N)^*$ $\bar{L}$. The traffic is assumed busty in nature, following a two-state discrete-time interrupted Poisson process (IPP). The IPP alternates between high (H) and low (L) traffic-arrival states per Frame_Time. IPP is characterized by four parameters $(\alpha, \beta, \lambda_H, \lambda_L)$, where $\alpha(\beta)$ is the probability of changing from state H (L) to L (H), and $\lambda_H(\lambda_L)$ represents the mean arrival rate at state H (L). The total numbers of data slots actually generated at the H (L) state follow the Poisson distribution with the mean arrival rate being equal to $\lambda_H(\lambda_L)$. Accordingly, $\bar{L}_o = [\beta/(\alpha+\beta)]\cdot\lambda_H + [\alpha/(\alpha+\beta)]\cdot\lambda_L$. Traffic burstiness B is defined to be the ratio of the peak arrival rate to the mean arrival rate. That is, $B = \lambda_H/\bar{L}_o$. In the simulation, we set: $\bar{L} = 0.9$, $\alpha = 0.25; \beta = 0.01$; and $B = 4$ to 10. Simulation results are shown in Fig. 3.

We first examine the impact of PQS on mean delay (in unit of frame) and delay fairness. As shown in Fig. 3(a), we observe a trade-off problem between mean delay and delay fairness. A smaller PQS setting $(=100)$ causes longer delay but attains superior delay fairness among all ONUs. Increasing the PQS (to 3000) effectively reduces the delay, however, at the expense of delay unfairness. The more downstream the ONU is located, the poorer delay it receives. The problem deteriorates under higher burstiness. Focusing on the positive effect, we examine the mean delay as a function of the PQS. As shown in Fig. 3(b), the mean delay decreases drastically with an increase in PQS. The greater the burstiness, the more delay improvement we achieve. The results in Fig. 3(b) provide useful guidelines on determining the PQS under a given traffic burstiness such that a delay requirement can be satisfied.

We then carried out the simulation of the neural-fuzzy MAC system [see Fig. 2(a)]. The objective is to determine the PQS and PR values for all ONUs, subject to satisfying a delay requirement and delay fairness for all ONUs. For the offline training, the simulation results from Fig. 3(a) and (b) are fed into the neural-fuzzy MAC system to perform the learning operation. The system parameters are given as: the fuzzy measurement $\mathrm{threshold} = 0.1$, where the higher value results in higher overlapping between fuzzy rules; learning $\mathrm{rate} = 0.005$; $\mathrm{F\_in} = 0.0001$, where the higher value corresponds to more rules to be generated; $\mathrm{F\_out} = 0.007$, where the higher value yields more output clusters to be generated. The overall training is performed with 50 000 iterations. For the online computation

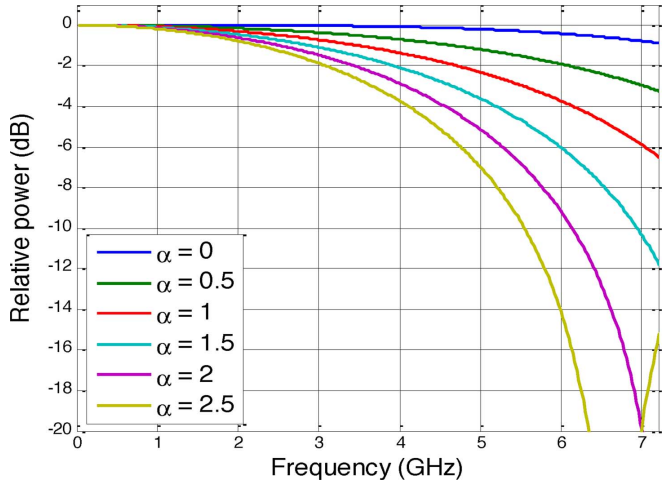

Fig. 5. Relative power of subcarriers after 20 km SMF transmission under different α's.

phase, we increase the learning rate to 0.01 and add forgetting $\text{factor} = 0.96$ to adapt to varying traffic conditions. Simulation results are shown in Fig. 4.

In the first experiment, we give a fixed PR $(=16)$ and a delay (between 5 and 40 Frame_Times) to the neural-fuzzy MAC system as inputs, and receive the corresponding PQS for each ONU as outputs. In Fig. 4, since the PQS values from ONU-1 to ONU-19 are the same as that of ONU-20, we only display the PQS results from ONU-20. We discover from Fig. 4(a) that, under any delay requirement, delay fairness is achieved by using larger PQS values for more downstream ONUs. The more stringent the delay requirement $(D = 5)$, the greater PQS the downstream ONUs require to achieve the same grade of delay as the upstream ONUs do. Moreover, as the delay requirement becomes highly stringent (5–10 Frame_Times), increasing the PQS is no longer doable for some most downstream ONUs. In the second experiment, we employ a fixed PQS (from 100 to 2000) and a high delay requirement $(D = 10)$, and receive the PR outputs from the neural-fuzzy system. We observe in Fig. 4(b) that the downstream ONUs require greater PR values to achieve the same delay requirement. The promising results in Fig. 4(b) show that the neural-fuzzy MAC system successfully guarantees a delay requirement and delay fairness by using different PR settings at different ONUs under various PQS values.

V. Theoretical Analysis of DML/EML Transmissions

In this section, we present a theoretical study on the physical impairments and penalty induced by DML/EML. Specifically, we mathematically represent the intensity modulated optical OFDM signal with positive chirp after modulation and transmission. Based on the analysis, we illustrate how power fading is mitigated by the pre-emphasis algorithm and the residual power penalty.

The OFDM signal with N subcarriers is expressed as $S = \sum_{n=1}^{N} s_n \cos(n\omega t + \theta_n)$, where ω is the subcarrier spacing, and s_n and θ_n are the encoded amplitude and phase information of the nth subcarrier, respectively. To zero in on the frequency chirp and dispersion behavior, we consider a simplified linear E/O model of DML/EML with no bandwidth limitation. Therefore, the output optical power is proportional to the modulation signal, which can be expressed, with a proper bias, as $P = P_0 + \eta S$, where P_0 is the bias optical power, and η is the slope of E/O conversion. Recall that the optical signal is generated in the form of the DSB; thus, the bandwidth of the optical OFDM signal becomes $2N\omega$. Moreover, the envelope of the output optical field can be given by $E = \sqrt{P_0 + \eta S} e^{-j\Delta\phi}$ [15], where $\Delta\phi$ is the addition phase modulation caused by the amplitude variation of the modulation signal and can be expressed as

$$\frac{d\phi}{dt} = \frac{\alpha}{2P}\frac{dP}{dt} \Rightarrow \Delta\phi = \frac{\alpha}{2}(\ln P - \ln P_0) \tag{3}$$

where α is the linewidth enhancement factor of DML/EML [16]. Using the small signal approximation of $\eta s_n \ll P_0$ with only the first order of s_n taken into consideration, the optical field is approximated as

$$\begin{aligned} E &\cong \sqrt{P_0}\left[1 + (1 - j\alpha)\sum_{n=1}^{N} x_n \cos(n\omega t + \theta_n)\right] \\ &= \sqrt{P_0}\left[1 + \sqrt{1+\alpha^2}\sum_{n=1}^{N} x_n \cos(n\omega t + \theta_n) e^{-j\theta_\alpha}\right] \end{aligned} \tag{4}$$

where $x_n = \eta s_n/(2P_0)$, and $\theta_\alpha = \tan^{-1}\alpha$. After fiber transmission of a distance L with the dispersion parameter β_2 and no fiber loss, the optical field given in (4) is added with the dispersion-induced phase shift $\theta_D = \beta_2 L\omega^2/2$, as

$$\begin{aligned} E_D(L) \cong \sqrt{P_0}\Bigg[1 + \sqrt{1+\alpha^2} \\ \times \sum_{n=1}^{N} x_n \cos(n\omega t + \theta_n) e^{j(n^2\theta_D - \theta_\alpha)}\Bigg]. \end{aligned} \tag{5}$$

At the receiver, after the square-law direct detection, the normalized received signal becomes

$$\begin{aligned} |E_D(L)|^2 \cong P_0\Bigg[1 + 2\sqrt{1+\alpha^2} \\ \times \sum_{n=1}^{N} x_n \cos(n\omega t + \theta_n)\cos(n^2\theta_D - \theta_\alpha)\Bigg] \end{aligned} \tag{6}$$

where the second order of x_n is omitted. Thus, the nth subcarrier power is proportional to

$$s_n^2(1+\alpha^2)\cos^2(n^2\theta_D - \theta_\alpha) \tag{7}$$

which under chirp free $(\alpha = 0)$ can be reduced to $s_n^2\cos^2(n^2\theta_D)$, the well-known formula of power fading [17]. As opposed to the chirp-free case, a positive α intensifies the power fading. In Fig. 5, we show the subcarrier power in (7) after 20 km standard SMF transmission. Clearly, the positive chirp results in reducing the transmission bandwidth of DML/EML-based optical OFDM signals. The higher the subcarrier frequency, the poorer the performance.

To compensate such power fading, we have designed a combinational employment of a pre-emphasis algorithm and adaptive subchannel modulation. The rationale behind the pre-emphasis algorithm is to homogenize the received SNRs across all subcarriers at the receiver by providing extra power for the subcarriers with poorer SNRs at the transmitter. The algorithm operates as follows. At the receiver, we periodically measure the SNR of all subcarriers, and calculate the pre-emphasis parameter as $p(n) = 10^{-(\rho_n - \bar{\rho}_n)/10}$, where ρ_n and $\bar{\rho}_n$ are the SNR's of the nth subcarrier with and without transmissions, respectively. Since SNR is a linear function of the power, and according to (7), we arrive at that $p(n)$ is closely in inverse proportion to $(1+\alpha^2)\cos^2(n^2\theta_D - \theta_\alpha)$. The amplitude level s_n for transmitted subcarrier n at the transmitter is, then, readjusted through multiplying it by the square root of its pre-emphasis parameter, i.e., $\sqrt{p(n)} \cdot s_n$. Accordingly, to maintain as high performance as that before the transmission, an additional optical power penalty is needed and approximated as

$$\frac{1}{N\sqrt{(1+\alpha^2)}} \sum_{n=1}^{N} |\sec(n^2\theta_D - \theta_\alpha)|. \tag{8}$$

Followed by pre-emphasis, we adopt adaptive subchannel modulation. As will be shown in the next section, we employ higher order and lower order QAM formats for the subcarriers with higher and lower SNRs, respectively.

VI. Experimental Setup and Results

In this section, we demonstrate via experimental results that VTOPS achieves 40 Gb/s downstream and upstream optical OFDM-signal transmissions by means of low-cost DML/EML devices. The experimental setup is shown in Fig. 6, with four corresponding electrical spectra displayed in the insets. As shown in Fig. 6, the experiment consists of three data flows: 1) OLT-Tx to ONU_1-Rx EML-based 20 km downstream; 2) ONU_1-Tx to ONU_2-Rx DML-based 5 km adjacent-ONU transmission; and 3) ONU_2-Tx to OLT-Rx EML-based 20 km upstream. While the downstream traffic from OLT to ONU_1 is carried via wavelength λ_d, the upstream traffic from ONU_2 to OLT is transported via λ_u.

At each of the three transmitters, OLT-Tx, ONU_1-Tx, and ONU_2-Tx, the OFDM signals are generated by an arbitrary waveform generator (AWG, Tektronix AWG7102) using the MATLAB program. The block diagram of the OFDM transmitter consists of serial-to-parallel conversion, QAM modulation, inverse fast Fourier transform (FFT), cyclic prefix (CP) insertion, and digital-to-analog conversion. The sampling rate and digital-to-analog converter resolution of the AWG are 12 GS/s and 8 bits, respectively. The OFDM signal is generated from two different OFDM bands (CH1 and CH2 in Fig. 6). In band 1 (CH1), the driving signal is based on a 128 QAM 23.4375-MSym/s symbol rate that is encoded at subcarriers 6–98 with a bandwidth of 2.18 GHz. This results in a total data rate of 15.2578 Gb/s. In band 2 (CH2), the OFDM signal is based on the same symbol rate but using 64 QAM. The signal is encoded and upconverted to 4.406 GHz occupying subcarriers 99–186 and subcarriers 200–287 constituting a total data rate of 24.75 Gb/s.

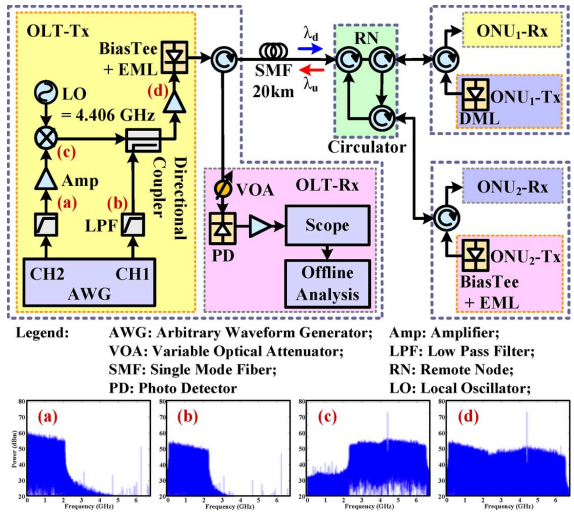

Fig. 6. Experimental setup with spectrum illustration. (a) 64 QAM CH2. (b) 128 QAM CH1. (c) CH2 after upconversion. (d) Combination of CH1 and CH2.

Since subcarrier-to-subcarrier interference is considerably low for a fiber transmission of 20 km [18], frequency guard band is unnecessary. Thus, with a total bandwidth of 6.305 GHz via the two OFDM bands, it is feasible to use inexpensive matured 10 GHz optical transceiver to achieve a total data rate of 40 Gb/s.

The signals from two bands are aggregated via a directional coupler and sent to the 10 GHz laser. While an EML is used at OLT-Tx and ONU_2-Tx, a DML is used at ONU_1-Tx. Namely, when EML is used, the experiment serves for testing the 20 km transmissions of downstream OFDM signal from OLT to ONU_1, or 20 km upstream transmissions from ONU_2 to OLT. When DML is used, the experiment serves for testing the 5 km transmission of OFDM signal from ONU_1 to ONU_2. Following standard 20 km (EML) or 5 km (DML) SMF transmission and through optical circulators in the RN, the optical OFDM signal is received via a 8.5 GHz PIN-type photodetector at any of OLT-Rx, ONU_1 -Rx, and ONU_2-Rx. A variable optical attenuator (VOA), which is used to emulate the additional optical loss, is passed through before the optical receiver. After square-law photo detection, a digital oscilloscope (Tektronix DPO 71254) captures the waveform based on a 50 GS/s sampling rate and a 3 dB bandwidth of 16 GHz. We, then, use an offline MATLAB DSP program to demodulate the OFDM signal. The demodulation process includes synchronization, FFT, one-tap equalization, and QAM symbol decoding. From the constellation of OFDM signals, we measure the SNR and, in turn, calculate the bit error rate (BER) [19].

As described in Section V, the unbalanced power-fading problem can be overcome by applying the pre-emphasis algorithm and adaptive subchannel modulation. As shown in Fig. 7, the blue curve corresponds to the results prior to pre-emphasis power adjustment. Though some subcarriers maintain relatively high SNR, the subcarriers located at high frequencies suffer from RF fading that causes severe SNR degradation. After applying the pre-emphasis algorithm, as shown in the red curve, we arrive at a smoother SNR curve and noticeable performance improvement. We then adopt adaptive modulation across two

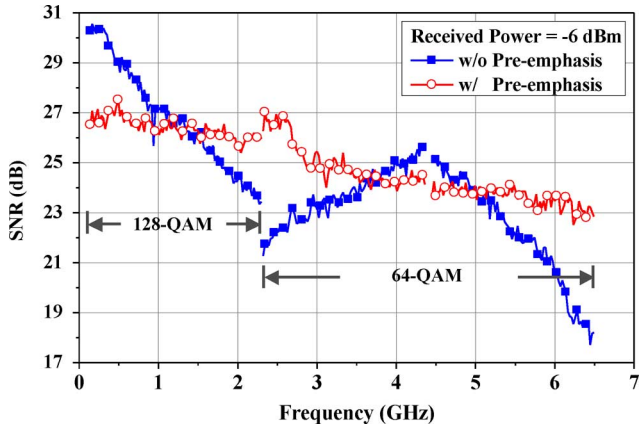

Fig. 7. Subcarrier SNR before and after pre-emphasis.

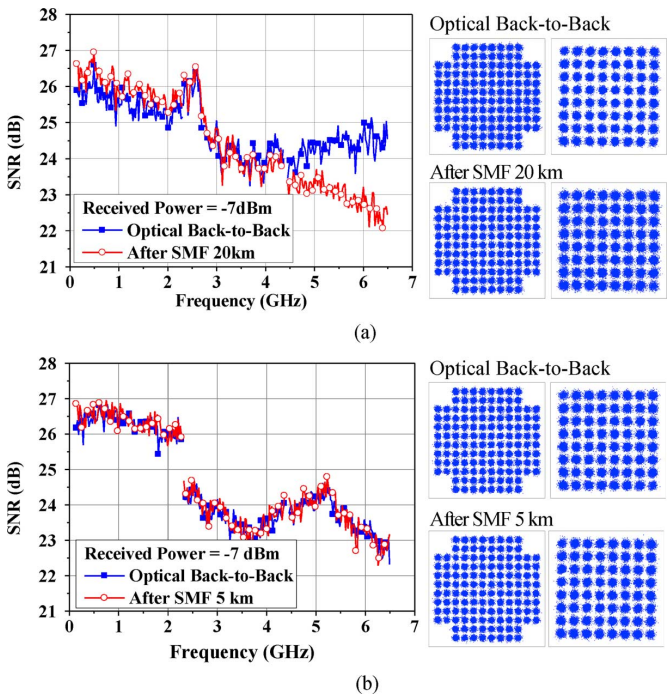

Fig. 8. SNR and constellation before and after fiber transmissions. (a) EML-based SNR and constellation. (b) DML-based SNR and constellation.

sets of subcarriers. As shown in the figure, we employ 128 QAM for band 1, and 64 QAM for band 2.

We depict in Fig. 8 the SNR of each subcarrier under back to back and following 20 km and 5 km SMF transmissions. The RF fading is intensified when combined with the frequency chirp from EA modulator [20]. After pre-emphasis, subcarriers at high frequencies receive better SNR as shown from the blue line of Fig. 8(a). However, after 20 km transmissions, due to RF fading, the higher frequency subcarriers undergo poorer SNR. We also plot the constellation diagrams for band 1 (12 QAM) and band 2 (64 QAM) before and after transmissions. We observe that, with adaptive subchannel modulation, clear constellations are maintained after transmissions under both EML and DML scenarios. Finally, we show in Fig. 9 the BER of DML and EML under back to back and following 5 km and 20 km SMF transmissions. Due to 5 km short-distance DML-based

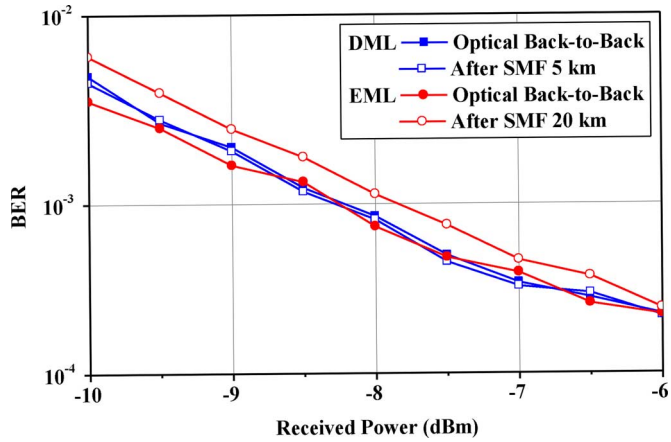

Fig. 9. BER of DML and EML before and after fiber transmissions.

transmissions, the BER after transmissions is as low as that before transmissions. Both DML and EML results show that we achieve a BER of less than 10^{-3} with acceptable receiving powers.

VII. Conclusion

In this paper, we have proposed a high-performance VTOPS. Coupled with the use of inexpensive direct modulation, DML/EML, VTOPS boasts several significant advantages including high scalability and spectrum efficiency. We also presented and implemented a neural-fuzzy rate-based MAC system for governing the dynamic and fair access of bandwidth over VTOPS. The neural-fuzzy MAC system dynamically returns the optimal PR and PQS values for all ONUs, satisfying the given delay requirement and achieving delay fairness across all ONUs under varying traffic conditions. We presented theoretical and experimental results to show that the unbalanced power-fading problem caused by the use of DML/EML can be effectively overcome by employing the pre-emphasis power-adjustment algorithm and adaptive subchannel modulation. Finally, experimental results show that, through optical circulators in the RN, VTOPS achieves 40 Gb/s downlink (20 km EML transmissions from OLT to the first ONU) and 40 Gb/s uplink (5 km DML transmissions between two adjacent ONUs, and 20 km EML from the last ONU to OLT).

References

[1] J. Kani, F. Bourgart, A. Cui, A. Rafel, M. Campbell, R. Davey, and S. Rodrigues, "Next-generation PON—Part I: Technology roadmap and general requirements," *IEEE Commun. Mag.*, vol. 47, no. 11, pp. 43–49, Nov. 2009.

[2] K. Grobe and J. P. Elbers, "PON in adolescence: From TDMA to WDM-PON," *IEEE Commun. Mag.*, vol. 46, no. 1, pp. 26–34, Jan. 2008.

[3] J. Armstrong, "OFDM for optical communications," *J. Lightw. Technol.*, vol. 27, no. 3, pp. 189–204, Feb. 2009.

[4] N. Cvijetic, D. Qian, and J. Hu, "100 Gb/s optical access based on optical orthogonal frequency-division multiplexing," *IEEE Commun. Mag.*, vol. 48, no. 7, pp. 70–77, Jul. 2010.

[5] Y. Lin and P. Tien, "Next-generation OFDMA-based passive optical network architecture supporting radio-over-fiber," *IEEE J. Sel. Areas Commun.*, vol. 28, no. 6, pp. 791–799, Aug. 2010.

[6] S. Chen, Q. Yang, Y. Ma, and W. Shieh, "Real-time multi-gigabit receiver for coherent optical MIMO-OFDM signals," *J. Lightw. Technol.*, vol. 27, no. 16, pp. 3699–3704, Aug. 2009.

[7] D. Qian, N. Cvijetic, J. Hu, and T. Wang, "A novel OFDMA-PON architecture with source-free ONUs for next-generation optical access networks," *IEEE Photon. Technol. Lett.*, vol. 21, no. 17, pp. 1265–1267, Sep. 2009.
[8] Z. Xu, M. O'Sullivan, and R. Hui, "OFDM system implementation using compatible SSB modulation with a dual-electrode MZM," *Opt. Lett.*, vol. 35, no. 8, pp. 1221–1223, 2010.
[9] Agiltron, Inc., Woburn, MA. [Online]. Available: http://www.agiltron.com/crystalatch_series F.htm
[10] M. Sugeno and K. Tanaka, "Successive identification of a fuzzy model and its applications to prediction of a complex system," *Fuzzy Sets Syst.*, vol. 42, no. 3, pp. 315–334, 1991.
[11] C. Lin and C. Lee, *Neural Fuzzy Systems: A Neuro-Fuzzy Synergism to Intelligent Systems*. Englewood Cliffs, NJ: Prentice-Hall, 1996.
[12] S. Horikawa, T. Furuhashi, and Y. Uchikawa, "On fuzzy modeling using fuzzy neural networks with the backpropagation algorithm," *IEEE Trans. Neural Netw.*, vol. 3, no. 5, pp. 801–806, Sep. 1992.
[13] Y. Lin and G. Cunningham, "A new approach to fuzzy-neural system modeling," *IEEE Trans. Fuzzy Syst.*, vol. 3, no. 2, pp. 190–197, May 1995.
[14] C. Juang and C. Lin, "An on-line self-constructing neural fuzzy inference network and its applications," *IEEE Trans. Fuzzy Syst.*, vol. 6, no. 1, pp. 12–32, Feb. 1998.
[15] J. Wang and K. Petermann, "Small signal analysis for dispersive optical fiber communication systems," *J. Lightw. Technol.*, vol. 10, no. 1, pp. 96–100, Jan. 1992.
[16] C. Henry, "Theory of the linewidth of semiconductor lasers," *IEEE J. Quantum Electron.*, vol. 18, no. 2, pp. 259–264, Feb. 1982.
[17] U. Gliese, S. Ngrskov, and T. Nielsen, "Chromatic dispersion in fiber-optic microwave and millimeter-wave links," *IEEE Trans. Microw. Theory Tech.*, vol. 44, no. 10, pp. 1716–1724, Oct. 1996.
[18] C. C. Wei, "Small-signal analysis of OOFDM signal transmission with directly modulated laser and direct detection," *Opt. Lett.*, vol. 36, no. 2, pp. 151–153, Jan. 2011.
[19] V. Urick, J. Qiu, and F. Bucholtz, "Wide-band QAM-over-fiber using phase modulation and interferometric demodulation," *IEEE Photon. Technol. Lett.*, vol. 16, no. 10, pp. 2374–2376, Oct. 2004.
[20] J. Wei, X. Jin, and J. Tang, "The influence of directly modulated DFB lasers on the transmission performance of carrier-suppressed single-sideband optical OFDM signals over IMDD SMF systems," *J. Lightw. Technol.*, vol. 27, no. 13, pp. 2412–2419, Jul. 2009.

Maria C. Yuang received the B.S. degree in applied mathematics from National Chiao Tung University (NCTU), Hsinchu, Taiwan, in 1978, the M.S. degree in computer science from the University of Maryland, College Park, in 1981, and the Ph.D. degree in electrical engineering and computer science from the Polytechnic Institute of New York University, Brooklyn, in 1989.

From 1981 to 1990, she was with AT&T Bell Laboratories and Bell Communications Research (Bellcore), where she was a member of technical staff and was involved in research on broadband networks and protocol engineering. In 1990, she joined NCTU, where she is currently a Professor in the Department of Computer Science and Information Engineering. She holds 20 patents in the field of broadband and wireless networking, and has more than 110 publications, and a book chapter. Her current research interests include broadband optical networks, data center networking, wireless local networks, and performance modeling and analysis.

Dr. Yuang has served as a Guest Editor for the Special Issue of the *IEEE Journal on Selected Areas in Communications* on next-generation broadband optical access network technologies in 2010. She has also served on the technical program committee of many international conferences including the IEEE International Conference on Communications and the IEEE Global Telecommunications Conference, and has been invited to give invited talks at numerous technical conferences. She is a member of the Optical Society of America.

Po-Lung Tien received the B.S. degree in applied mathematics, the M.S. degree in computer and information science, and the Ph.D. degree in computer science and information engineering, from National Chiao Tung University, Hsinchu, Taiwan, in 1992, 1995, and 2000, respectively.

In 2005, he joined National Chiao Tung University, where he is currently an Associate Professor in the Department of Electrical Engineering. His current research interests include optical networking, computational intelligence, network optimization, multimedia communications, and performance modeling.

Dar-Zu Hsu received the B.S. degree in communications engineering from National Chiao Tung University, Hsinchu, Taiwan, and the M.S. degree in electrical engineering from National Cheng Kung University, Tainan, Taiwan, in 1998 and 2000, respectively. He is currently working toward the Ph.D. degree in electro-optical engineering at National Chiao Tung University.

In 2000, he joined the Information and Communications Research Laboratories, Industrial Technology Research Institute, Hsinchu, where he is currently a Deputy Manager of Optical Communications and Networking Technology Department. He is also with the Department of Photonics, National Chiao Tung University. His research interests include passive optical networks and optical orthogonal frequency-division multiplexing transmission systems.

Shing-Yu Chen received the B.S. degree in electro-physics and the M.S. degree in electro-optical engineering from National Chaio Tung University, Hsinchu, Taiwan.

He is currently with the Optical Communications and Networking Technology Department, Information and Communications Research Laboratories, Industrial Technology Research Institute, Hsinchu. His research interests include passive optical networks and optical orthogonal frequency-division multiplexing transmission systems.

Chia-Chien Wei received the Ph.D. degrees in electro-optical engineering from National Chiao Tung University, Hsinchu, Taiwan, and in electrical engineering from the University of Maryland, Baltimore, in 2008.

In 2011, he joined National Sun Yat-sen University, Kaohsiung, Taiwan, where he is currently an Assistant Professor in the Department of Photonics. His current research interests include optical and electrical signal processing, advanced modulation formats, optical access networks, and radio-over-fiber systems.

Ju-Lin Shih received the Ph.D. degree in computer science and information engineering from National Chiao Tung University, Hsinchu, Taiwan, in 2006.

From 2006 to 2011, he was with National Chiao Tung University, where he was a Postdoctoral Fellow in the Department of Computer Science and Information Engineering. In 2011, he joined the Compal Communications, Inc., Taipei, Taiwan, where he is currently involved in research on mobile networks and protocol engineering. His research interests include high-speed networking, optical networking, wireless local networking, mobile communications, and performance modeling and analysis.

Jyehong Chen received the B.S. and M.S. degrees in electrical engineering from National Taiwan University, Taipei, Taiwan, in 1988 and 1990, respectively, and the Ph.D. degree in electrical engineering and computer science from the University of Maryland, Baltimore, in 1998.

In 1998, he joined JDS Uniphase Corporation as a Senior Engineer and received 10 U.S. patents in two years. He joined the faculty of National Chiao Tung University, Hsinchu, Taiwan, in 2003, where he is currently a Professor at the Institute of Electro-Optical engineering and Department of Photonics. He has published more than 100 papers on international journals and conferences. His research interests include hybrid access network, long-reach passive optical network, and optical interconnects.